Preprints, 4th IFAC Conference on
Advances in Proportional-Integral-Derivative Control
Almería, Spain | June 12-14, 2024

Analysis and design of PI-based controllers for the axes of European Solar Telescope

Airam Ramirez-Cabrera * **Jose M. Gonzalez-Cava** *
Javier Leon-Gil ** **Nicolas Rodriguez-Linares** **
Miguel Nuñez-Cagigal ** **Juan A. Mendez-Perez** *

* *Departamento de Ingeniería Informática y de Sistemas, Universidad de La Laguna, La Laguna 38200, Tenerife, Spain (e-mail: jgonzalc@ull.edu.es).*
** *Instituto de Astrofísica de Canarias (IAC), Calle Vía Láctea s/n, 38205 La Laguna, Tenerife, Spain.*

Abstract: European Solar Telescope (EST) represents the largest European research infrastructure projected in the field of solar astrophysics. It is a 4-meter class solar telescope currently in the design phase. Within this phase, an essential objective is to analyze the control strategy of the telescope axes to achieve an accurate sun trajectory tracking. This paper presents a cascade control scheme based on proportional-integral (PI) controllers specifically designed for the elevation and azimuth axes of EST. The control strategy, which employs nested position-velocity loops, is devised to adeptly track the sun's trajectory while mitigating wind impact. The controller tuning adheres to criteria of relative stability margins and bandwidth constraints using the state-space representation derived from Finite Element Model of the EST structure. An end-to-end dynamics model has been proposed to evaluate the performance of the control strategy during a ten-minute simulation. Results evidenced the convenience of the proposed controllers, highlighting wind as the main source of the control error (0.78 arcsec and 0.14 arcsec in azimuth and elevation axes, respectively) compared to the sun tracking error. Future control strategy enhancements should target the reduction of wind-induced effects to meet stringent image stability requirements.

Keywords: Axis Control Strategy; Cascade control; End-to-end model; European Solar Telescope; PI controller; Wind rejection.

1. INTRODUCTION

European Solar Telescope (EST) is a project aimed at studying the magnetic connectivity of the solar atmosphere, from the deep photosphere to the upper chromosphere. With its 4.2 m primary mirror and an open configuration, EST will become the most powerful European ground-based facility to study the Sun in the coming decades in the visible and near-infrared bands (Noda et al. (2022)). EST uses the most innovative technological advances to overcome current observational limitations of existing facilities. The telescope will include the first adaptive secondary mirror ever used in a solar telescope (Kuiper et al. (2022)). In addition, a Multi-Conjugated Adaptive Optics (MCAO) system will compensate for the atmospheric turbulence (Femenía-Castella et al. (2022)). The primary mirror will allow for correcting its own surface figure errors due to slow-shift effects as well as piston and tip-tilt corrections (Ángel Mato Martínez et al. (2022)).

The design of EST must adhere to stringent requirements to ensure compliance with scientific specifications. This imperative requires minimizing tracking errors, which forces the system to achieve a high degree of stiffness. This high stiffness is essential to restrict image motion and control the modal behavior of both the telescope structure and pier (Cózar-Castellano et al. (2022)). The telescope structure must provide a pointing accuracy of $\pm 2.7''$ and a solar tracking error of $\pm 0.9''$. Note that EST will conduct observations in an open enclosure configuration to enhance natural airflow. The main challenge lies in the exposure to wind loads on the telescope structure, which especially affect the primary and secondary mirrors. This makes it necessary the development of a control strategy capable of tracking the sun trajectory while limiting the effect of wind shaking over the elevation and azimuth axes.

A frequently suggested control architecture for telescope axis control is the cascade position-velocity design, in which individual controllers must be tuned for each axis. The optical and mechanical design of the telescope determines the inertia of the telescope itself, which plays a crucial role in the control strategy. The inertia of the motors and the combined stiffness between the telescope structure and the stiffness of the gear trains are key factors consider in the control problem (Kärcher (2021)). PID-based controllers have been widely used in this field. A PI controller for both position-velocity loops was proposed in Sedghi et al. (2010) as baseline design to compute the telescope performance of main axes control for E-ELT. A PWM-based PI controller in Kumar and Banavar (2013) was also used for the axes control for the 50/80 cm Schmidt

telescope. The proposed controller showed a reasonably good performance during tracking operations. Optimal PID controllers also ensured accurate pointing and tracking for the 50cm robotic telescope (Stanzin et al. (2022)). Alternative proposals have relied on LQG controllers to suppress the telescope vibrations when PI controller gains are increased. TNG telescope has analysed the feasibility of implementing an LQG including an estimator of the structure flexible modes. The tracking version of the LQG controller resulted in a PI augmented with a flexible mode controller, where the increase of the proportional gain cause no longer instability because vibrations are suppressed (Schipani et al. (2020)).

The main contribution of this article focuses on proposing and analyzing a Proportional-Integral (PI) controller for the axes control of EST during tracking operations. Specifically, the suitability of this type of controller in a nested position-velocity structure for the elevation and azimuth axes will be examined. To achieve this, the tuning of the controller will be based on a frequency analysis of the telescope structure obtained from the Finite Element Model (FEM) proposed in the preliminary design phase of EST. Additionally, to assess the performance of the algorithm, the development of a Simulink end-to-end model is proposed tp evaluate the temporal response of the system to address two main challenges: i) solar tracking, ii) wind effect reduction during tracking trajectory. The simulation will analyze a specific case based on an early morning observation due to its high scientific interest motivated by low local seeing degradation.

This article is structured as follows. First, the control problem to be addressed for EST is introduced. Then, Section 3 outlines the methods used to propose and simulate the control strategy. Section 4 presents the simulation results obtained. Finally, the main conclusions of this work are presented.

2. PROBLEM STATEMENT

The main objective of telescope axis control involves addressing two key problems: a servo problem, associated with accurate tracking of the sun's trajectory during the observation period; and a regulator problem, associated with mitigating the impact of wind on the telescope surface, which introduces image motion. To achieve this, the system is equipped with a set of sensors and actuators designed to minimize control errors. Fur encoder heads an a encoder tape will be installed on each axis for feedback control. Additionally, elevation axis will be equipped with two direct drive motors, while one direct drive motor will be installed on the azimuth axis. In the current EST design, a co-located system has been assumed. In co-located systems, actuators and sensors are placed together, or joined by a stiff element, so that no relative deformation is introduced between them. This scheme comes with the advantage of pole-zero interlacing, so that the system becomes stable (see Preumont (1999)). Otherwise, non co-located systems are much more sensitive to perturbations, which results in stability degradation.

Apart from the rigid body motion introduced by the wind, deflections of the structure also occur. However, this effect is not initially computed in the closed-loop control of the axes. Therefore, the telescope axis control system should incorporate feedback information from another telescope subsystem to provide image motion corrections derived from the focal plane. Thus, given the nature of this control system, it will play a crucial role in correcting image motion that requires large ranges of movements at very low temporal frequencies.

The convenience of the controller structure and the tuning process for the axis control of a telescope will be conditioned by its mechanical design (primarily affecting resonance modes) and the proposed scientific requirements. The objective of this study is to analyze the performance of a cascade position-velocity structure for the elevation and azimuth axes. A PI-type controller will be proposed for each axis. The suitability to address trajectory tracking and wind disturbance rejection is assessed. In this study, the control error achieved over ten minutes will be simulated, according to the tracking requirement defined for EST.

To include the effect of wind, the wind model developed by the European Solar Telescope Project Office in Gonzalez-Cava et al. (2022) has been employed. This model is based on a Power Spectral Density (PSD) fitted using real data measured at a site close to where EST will be located, at the Observatorio del Roque de los Muchachos (La Palma, Spain). Specifically, this model is based on a four-segment PSD on the form

$$S_g(f) = A \cdot f^B \tag{1}$$

where S_g is the PSD, A represents the magnitude, B quantifies the slope and f is the linear frequency.

A Matlab code developed by the European Solar Telescope Project Office was used to generate the sun trajectory. This code generates the elevation and azimuth angles for solar tracking based on the proposed EST location.

Specifically, this work proposes the performance evaluation of the PI-based control strategy for an elevation-azimuth configuration considering an early morning observation. This scenario is of special scientific interest since local seeing effects are limited. A starting angle of 4.8° for elevation and 120.2° for azimuth (telescope pointing East) is proposed. As for the wind direction, preliminary analyses highlighted that the worst configuration corresponds to sideward wind (Soler et al. (2022)), so this scenario has been considered in the simulations.

3. METHODS

3.1 Dynamic model of EST structure

The dynamic model considered in this work is based on the preliminary design of European Solar Telescope. The EST Telescope Mount adopts a gantry-type telescope, which is further divided into the elevation axis and the azimuth axis. The elevation structure provides support for the secondary mirror and the heat rejecter. The design of the telescope mount structure prioritizes meeting the required stiffness, taking into account eigenfrequency requirements and adhering to the maximum allowable deflection of the optical unit to minimize image motion.

The telescope model has been created in Ansys/Mechanical. The telescope model comprises the azimuth structure, the elevation structure, and the optical components. The elevation structure was built using a combination of beam and shell elements. The primary mirror assembly is represented as a rigid body, incorporating its geometric shape and mass properties. The secondary mirror is simulated as a rigid beam element with a circular cross-section and representative mass, attached to the elevation structure through rigid beam elements. The heat rejecter is modeled as a point mass, strategically positioned at the intersection of the four supporting beams for the heat rejecter. Ansys/Mechanical allows state-space matrices to be exported from the modal analysis. Since the stiffness of the telescope is influenced by the elevation and azimuth angles, the modal solution, and hence the state-space matrix must be updated when large deviation in the elevation angle are expected. Since this study focuses on a ten-minutes trajectory, low elevation angle variations are expected so that the same state-space representation can be kept throughout the simulation.

In the field of structural engineering, the motion of a discrete dynamic system can be defined by equation (2).

$$[M]\{\ddot{u}\} + [C]\{\dot{u}\} + [K]\{u\} = \{F\} \tag{2}$$

M, C and K are the mass, damping and stiffness matrices, respectively; F is the load vector, and u, $\dot{u}$, and $\ddot{u}$ are the system response in terms of nodal displacements, velocities and accelerations, respectively.

Finally, state-space matrices of equation (3) can be extracted from the modal superposition analysis (see Gonzalez-Cava et al. (2022)).

$$\begin{aligned} \dot{z}(t) &= [A]z(t) + [B]i(t) \\ o(t) &= [C]z(t) + [D]i(t) \end{aligned} \tag{3}$$

A, B, C and D are the state-space matrices, $i(t)$ represents the force inputs and $o(t)$ represents the output elevation and azimuth rotations. Three inputs were considered for the state-space model: i) wind load over the structure, ii) force applied by the elevation drives, and iii) force applied by the azimuth drive. Inputs were defined in ANSYS by using unitary forces for the drives, and a pressure with a unitary wind speed for the wind load. The wind load was defined as a pressure p that depended on the wind speed as given by $p = 0.5\rho CDV^2$, where ρ is the air density, CD is the drag coefficient, and V is the wind speed. Drives force was applied at the nodes where they will be installed. Two outputs representing the elevation and azimuth rotations measured by the encoders were considered.

The frequency response of the system when considering an elevation angle of 6^{o} and lateral wind is depicted in the Bode diagram in Fig. 1. State-space representation obtained from modal analysis consisted of the first 500 resonant modes (1000 states) to have a modal mass $> 95\%$ of the total structure mass. Model reduction based on truncation has been proposed to reduce computational cost during controller tuning and simulation. In this study, the first 10 resonant modes (20 states) of the telescope structure have been considered sufficient to include the maximum resonant peak observed in the Bode magnitude response.

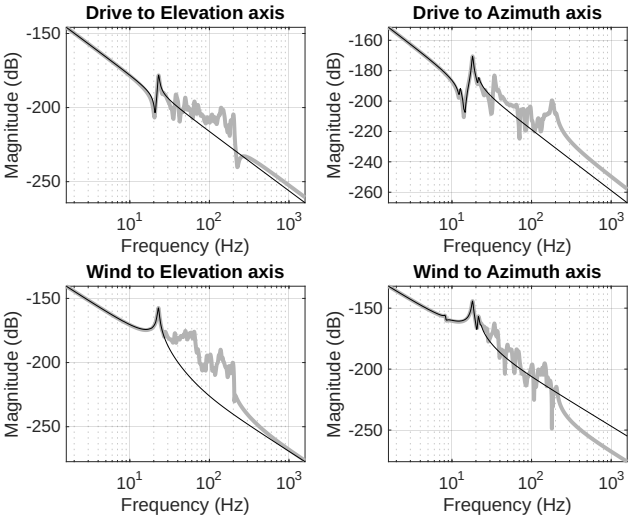

Fig. 1. Bode plot (magnitude, in dB) for the telescope structure. The original system is represented in gray, while the reduced model is depicted in black.

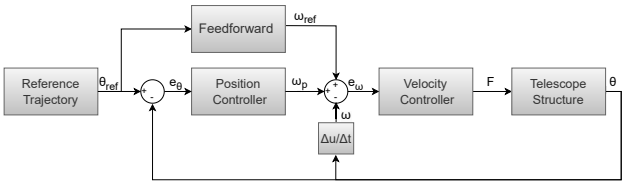

Fig. 2. Block diagram of the closed-loop system. The signals are: position reference, θ_{ref}; position error, e_θ; telescope position, θ; feedforward velocity term, ω_{ref}; velocity reference from position controller, ω_p; velocity error, e_ω; Force, F; telescope velocity, ω.

3.2 Controller design

For the control of each axis, a nested control architecture is proposed, as depicted in Fig. 2. The preliminary design of the EST structure allows considering negligible coupling between elevation and azimuth axes, leading to the independent tuning analysis of each axis. The control structure will consist of an outer position loop which sets the setpoint of an inner velocity loop. Thus, while the velocity loop (fast loop) will focus on minimizing the impact of wind disturbances on the trajectory, the primary role of the position loop (slow loop) will be to perform reference tracking. Note that the preliminary design of the EST structure is equipped with position encoders only. Therefore, their derivatives will be obtained mathematically to quantify the velocity feedback for the inner loop. As a general criterion, efforts will be made to minimize interactions between the velocity loop (higher bandwidth, faster response) and the position loop by establishing a bandwidth ratio constraint between both loops. Additionally, a feedforward term will be included in the velocity loop based on the position reference.

The locked rotor frequencies limit the bandwidth of the corresponding controller design. To avoid self-excitation of the resonance modes of the structure through the axis

control, a limitation is imposed on the bandwidth of each axis. Specifically, the maximum achievable bandwidth for the fastest loop (velocity loop) is proposed to be one-third of the first resonance peak. For satisfactory performance, a phase margin (PM) greater than 30°, and a gain margin (GM) greater than 6dB is also proposed to guarantee stability as generally recommended in the literature.

First, the velocity-loop controller is tuned. A controller on the form of equation (4) is considered. The second-order filter allows for additional attenuation in case the gain peak at the first resonance frequency should be attenuated to prevent for system response degradation.

$$\begin{aligned} K(s) &= C(s)F(s) \\ C(s) &= K_p + K_i\frac{1}{s} \\ F(s) &= \frac{w_n^2}{s^2 + 2\delta w_n s + w_n^2} \end{aligned} \tag{4}$$

For the position loop, a proportional controller $C(s) = K_p$ is proposed as sufficient to achieve zero steady state error under the conditions analyzed. The tuning of the position loop will take into account the bandwidth limitation derived from the velocity loop. Finally, the resulting controllers will be discretized for the simulation. For this purpose, a first-order hold (FoH) will be employed, considering a sampling frequency of $100Hz$ compatible with the expected values for the EST equipment.

3.3 Simulation tool

To analyze the results of the control strategy, an end-to-end model based on the time response of the closed-loop structure is analyzed. This model allows verifying the tests trajectories proposed in this study. A Simulink model is proposed to that end. The general structure of the model is depicted in Fig. 3.

The Trajectory block computes the elevation and azimuth references, while the Wind block generates the temporal wind signal based on the wind PSD model. The control system includes the state-space representation of the elevation and azimuth axes, as well as the proposed controller for each axis. Finally, the error block calculates the static error component (mean error), the dynamic error component (standard deviation) and the total error (root mean squared error, RMSE).

This Simulink model will compute the static and dynamic error components over a 10-minute simulation according to the tracking error requirement defined for EST. Three different scenarios will be studied: i) sun tracking without wind disturbance, ii) disturbance rejection for a constant setpoint, and iii) a combination of wind disturbance and sun tracking. The proposal of these scenarios will allow to identify the main component of the error and its contribution to the total error computation. Note that the application of the wind disturbance at the beginning of the simulation will introduce a fictitious excitation of the vibration modes of the structure due to the mean wind component, which is similar to a step input of magnitude $12.3m/s$. To avoid this effect, an initial stage is proposed in which a constant wind of 12.3 m/s is applied. Once the system reaches steady state due to the effect of mean wind, the dynamic wind component is applied for the control error computation.

4. RESULTS

4.1 Controllers tuning

The controller parameters were manually tuned, taking into account the resulting frequency response as well as the time evolution of the tracking error. First, the tuning of the controller for the azimuth structure was addressed. According to the Bode plot in Fig. 1, the maximum resonant peak for the azimuth structure occurs at 18 Hz. Consequently, the attempted closed-loop bandwidth of the velocity loop was set at 6 Hz. Initially, proportional and integral gains were adjusted to satisfy relative stability criteria. Amplification of the resonant peak was evident in the open-loop response. Consequently, a second-order filter was introduced in series to mitigate this effect. Finally, parameters of the considered filtered PI were $K_p = 4.8{\cdot}10^6$, $K_i = 2.9 \cdot 10^7$, $\delta = 0.8$ and $\omega_n = 40.8rad/s$. Relative stability margins were PM = 49.3° and GM = $7.5dB$. An example of the open-loop frequency response used for computing phase margin and gain margin is shown in Fig. 4. The closed-loop bandwidth was $6.1Hz$.

Subsequently, the position controller was fine-tuned. In addition to meeting to relative stability criteria, the position controller was adjusted to limit the closed-loop bandwidth of the position loop to a maximum of 2 Hz. This limitation aimed to minimize interactions with the inner loop. Finally, the position controller was set to $K_p = 4.6$. Relative stability margins were PM = 75.3° and GM = $13.1dB$. Closed-loop bandwidth for the position loop was $1.97Hz$.

The controller for the elevation structure was tuned likewise. The velocity loop bandwidth was set to approximately $7.3Hz$. Similar to the azimuth axis control case, a second-order filter in series was proposed to attenuate the effects of the resonance peak at $22Hz$. The parameters of the resulting filtered PI were $K_p = 2.9 \cdot 10^6$, $K_i = 3.0 \cdot 10^7$, $\delta = 0.8$ and $\omega_n = 56.6rad/s$. Relative stability margins were PM = 43.3° and GM = $8.9dB$. Closed-loop bandwidth of the velocity loop was $7.3Hz$.

The position controller for the elevation axis was adjusted to constrain the closed-loop bandwidth, aiming to minimize interactions with the inner loop. Finally, the position controller was set to $K_p = 5.2$. Relative stability margins were PM = 82.4° and GM = $12.8dB$. The closed-loop bandwidth for the position loop was $2.6Hz$. Bode plots of the resulting closed-loop systems for the position control of the azimuth and the elevation axes are presented in Fig. 5.

4.2 Simulation results

For the simulation of the results, the three proposed scenarios described in Section 3.3 have been evaluated using the Simulink model. An elevation and azimuth reference trajectory corresponding to a morning observation has been applied. The time-domain signal for the wind disturbance has been obtained from the wind model developed for EST. An example of the temporal evolution of the position for the azimuth and elevation axes for scenario iii), as well as the control error over a 10-minute period, is

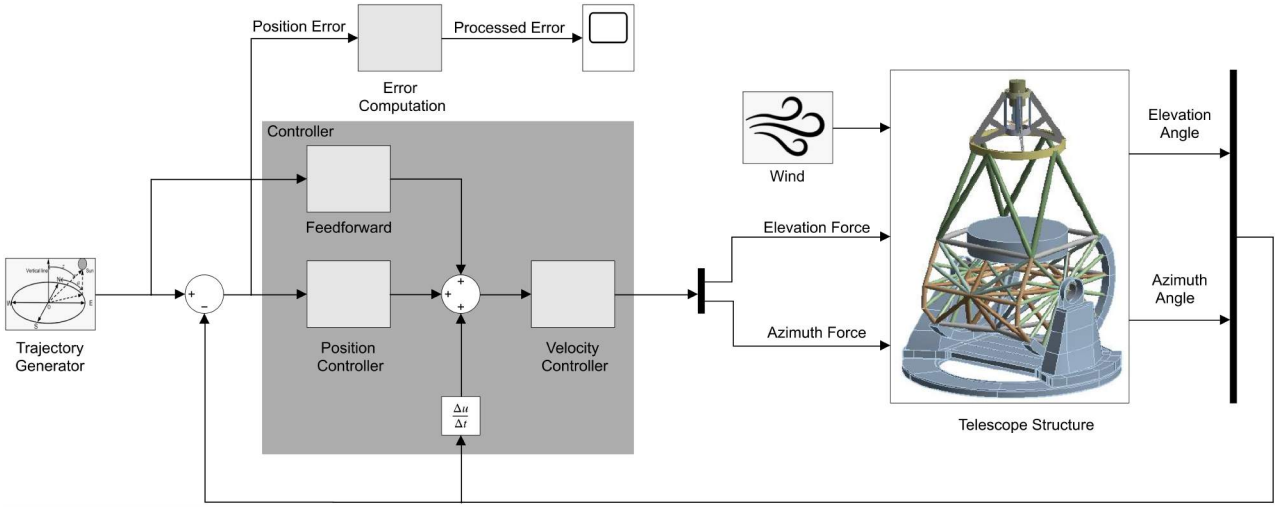

Fig. 3. Caption of the Simulink end-to-end model developed to compute the control error.

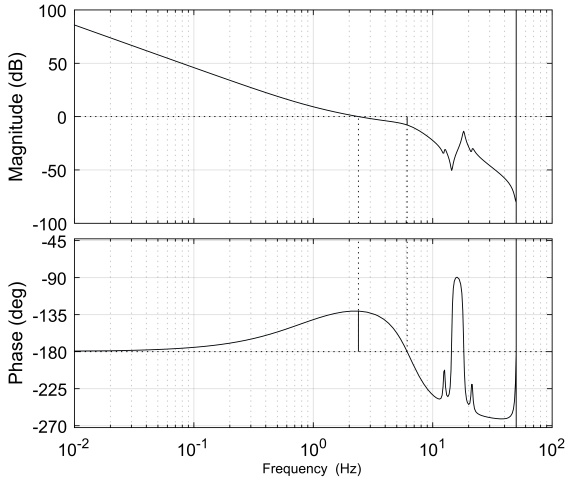

Fig. 4. Bode plot of the open-loop response of the velocity loop for the azimuth structure. Phase and Gain margins represented in vertical lines.

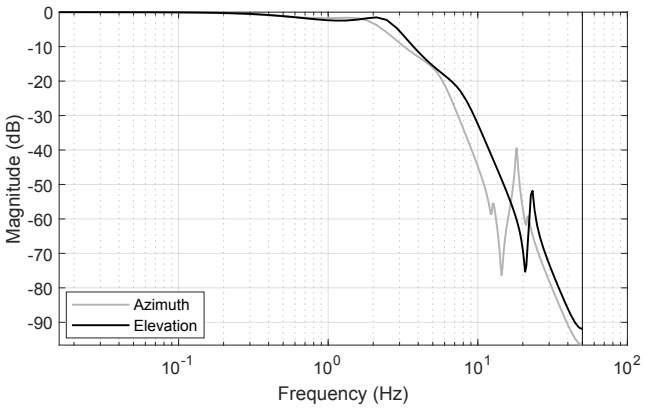

Fig. 5. Bode plot (magnitude) of the closed-loop response of the position loop for the azimuth and the elevation structures.

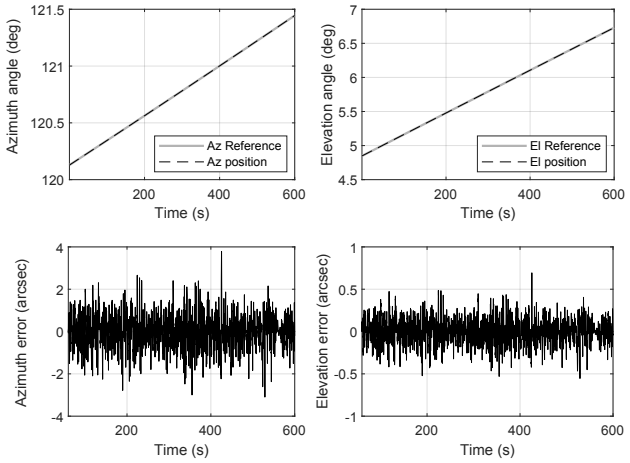

Fig. 6. Evolution of the azimuth (top left) and elevation (top right) angles and control errors (bottom) considering effects of wind disturbance and sun tracking.

depicted in Fig. 6. The results related to the position control error for the azimuth and elevation axes are presented in Table 1 and Table 2, respectively.

Table 1. Simulation results (in arcsec) for the Azimuth axis

	Mean Error	Dynamic Error	RMSE
Reference Tracking (Wind = $0m/s$)	$2.5 \cdot 10^{-11}$	$9.6 \cdot 10^{-6}$	$9.6 \cdot 10^{-6}$
Wind Rejection (Setpoint = $0rad$)	$7.6 \cdot 10^{-4}$	0.78	0.78
Reference Tracking + Wind Rejection	$7.6 \cdot 10^{-4}$	0.78	0.78

The results demonstrate that the proposed cascade control schemes, based on the use of PI controllers, are able to address both reference tracking and mitigate the effects of wind on the EST telescope structure. It is worth noting that the main source of control error is introduced by the wind regardless the axis. Specifically, the highest errors are observed in the azimuth axis (0.78 arcsec). This is attributed to the analyzed configuration, in which a lateral

Table 2. Simulation results (in arcsec) for the Elevation axis

	Mean Error	Dynamic Error	RMSE
Reference Tracking (Wind = $0m/s$)	$1.5 \cdot 10^{-5}$	$7.6 \cdot 10^{-4}$	$7.6 \cdot 10^{-4}$
Wind Rejection (Setpoint = $0rad$)	$1.3 \cdot 10^{-4}$	0.14	0.14
Reference Tracking + Wind Rejection	$1.4 \cdot 10^{-4}$	0.14	0.14

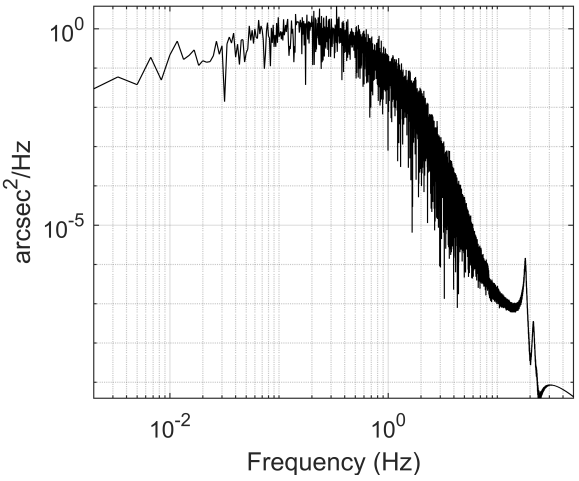

Fig. 7. Power spectral density of the control error for the azimuth axis.

wind is applied, leading to more pronounced effects on the azimuth axis. Considering the power spectral density of the wind model, the power is mainly concentrated at low frequencies ($< 1Hz$). This is also evident in the PSD of the control error (see Fig. 7). One potential alternative for reducing this control error would be to increase the system's bandwidth, leading to greater attenuation of low-frequency components in the system's sensitivity curve, S. However, this would come at the expense of reducing the bandwidth ratio between the velocity and position loops (currently around a factor of 3).

In this study, a single telescope pointing configuration has been analyzed. The same procedure could be applied to different configurations of interest in order to characterize the maximum control error. It is worth noting that this would involve generating the state-space representation for each configuration under analysis. In addition, further research should include new elements to the control scheme, such as the effects of the drives (cogging and ripple torques), bearings (friction effects) and encoders.

5. CONCLUSION

In this paper, a control scheme based on a proportional-integral controller has been proposed for the control of the elevation and azimuth axes of European Solar Telescope. For this purpose, a cascade position-velocity control has been implemented. An end-to-end model has been developed to assess the performance of the control strategy. Initially, the tuning of the different controllers has been proposed based on relative stability and bandwidth criteria. To accomplish this, the state-space representation of the EST structure derived from FEM analysis has been employed. Finally, the simulations have demonstrated the capability of such controllers to effectively control the axes of the current design of European Solar Telescope. The ability of the control system to i) track the sun trajectory, and ii) reject the effects of the wind disturbance has been evaluated. The analysis has shown that wind disturbance is the main component of the control error in the current scenario. Future advances in the control strategy should focus on mitigating the impact of this component to ensure the fulfillment of the scientific requirements for image stability.

REFERENCES

Cózar-Castellano, J., Cagigal, M.N., Vega, N., Mato, A. et al. (2022). Overview of telescope structure, enclosure, and pier preliminary design of the european solar telescope. 57. SPIE. doi:10.1117/12.2629629.

Femenía-Castella, B., Cagigal, M.A.N., Barreto, M., Belío-Asin, M. et al. (2022). Adaptive optics at the european solar telescope: status and future developments. 71. SPIE. doi:10.1117/12.2629516.

Gonzalez-Cava, J.M., Soler, M., González, F., Cózar-Castellano, J. et al. (2022). Dynamic modeling, control and simulation of the est telescope structure: quantifying performance during tracking operation. 71. SPIE. doi:10.1117/12.2628247.

Kuiper, S., Bos, A., de Vreugd, J., Witvoet, G. et al. (2022). Preliminary design of the adaptive secondary mirror for the european solar telescope. 80. SPIE. doi:10.1117/12.2629495.

Kumar, T.S. and Banavar, R.N. (2013). Design and development of telescope control system and software for the 50/80cm schmidt telescope. *Optical Engineering*, 52, 081607. doi:10.1117/1.OE.52.8.081607.

Kärcher, H.J. (2021). From main axes control to flexible body control of large telescope structures. *Advanced Control for Applications*, 3. doi:10.1002/adc2.88.

Noda, C.Q., Schlichenmaier, R., Rubio, L.R.B., Löfdahl, M.G. et al. (2022). The european solar telescope. *Astronomy and Astrophysics*, 666, A21. doi:10.1051/0004-6361/202243867.

Preumont, A. (1999). Vibration control of active structures: An introduction. *Meccanica*, 34, 139–139. doi:10.1023/A:1004398914135.

Schipani, P., Gonzalez, M., Perrotta, F., Savarese, S. et al. (2020). Towards new servo control algorithms at the tng telescope. 209. SPIE. doi:10.1117/12.2560498.

Sedghi, B., Müller, M., Erm, T., Brunetto, E. et al. (2010). Main axes control of e-elt. 77331G. doi:10.1117/12.856871.

Soler, M., Cózar-Castellano, J., Ángel Mato, Ferro, I. et al. (2022). Structural analysis for the est preliminary design specifications. 41. SPIE. doi:10.1117/12.2628912.

Stanzin, T., Jorphail, S., Parihar, P., Angchuk, D. et al. (2022). The 50cm robotic telescope: control system upgrade and automation. 12. SPIE. doi:10.1117/12.2629134.

Ángel Mato Martínez, Vega, N., Soler, M., Cozar-Castellano, J., Gonzalez-Cava, J.M., et al. et al. (2022). M1 assembly for the est: selection of the most promising baseline configuration for the preliminary design. 10. SPIE. doi:10.1117/12.2628568.